Biophysical Journal, Volume *119*

Supplemental Information

Determining the Stoichiometry of Small Protein Oligomers Using Steady-State Fluorescence Anisotropy

Philipp J. Heckmeier, Ganesh Agam, Mark G. Teese, Maria Hoyer, Ralf Stehle, Don C. Lamb, and Dieter Langosch

SUPPORTING MATERIAL

Three Supplementary Figures (S1-S3) provide additional information on the fusion proteins investigated in this study, two Supplementary Figures (S4 and S5) describe details of how fluorescent samples were analyzed via time-resolved methods, and the last Supplementary Figure (S6) shows the approach of characterizing sf-GFP-ph3a by total internal reflection fluorescence (TIRF) microscopy.

Figure S1: 1xGFP amino acid sequence and plasmid construct.

Figure S2: The shape of GFP concatemers determined from FCS measurements in solution.

Figure S3: Size exclusion chromatography profiles of different GFP-coiled-coil fusion proteins.

Figure S4: Determination of the homotransfer rate k_{FRET} from time-resolved anisotropy decays.

Figure S5: Exemplary fit to the fluorescence lifetime decay.

Figure S6: TIRF microscopy based direct photobleaching of sfGFP-ph3a.

The Supporting Material further comprises two Supplementary Tables.

Table S1: Determination of protein stoichiometry N from fluorescence anisotropy using authentic versus crosswise standardized parameters.

Table S2: Diffusion coefficients of sfGFP-GCN4-p1 and sfGFP-GCN4-pII constructs.

In the last section “Supplementary Theory – Fractional Photobleaching”, we give details on the approach to characterize the stoichiometry of protein oligomers via steady-state anisotropy in combination with fractional photobleaching.

Supplementary Figures

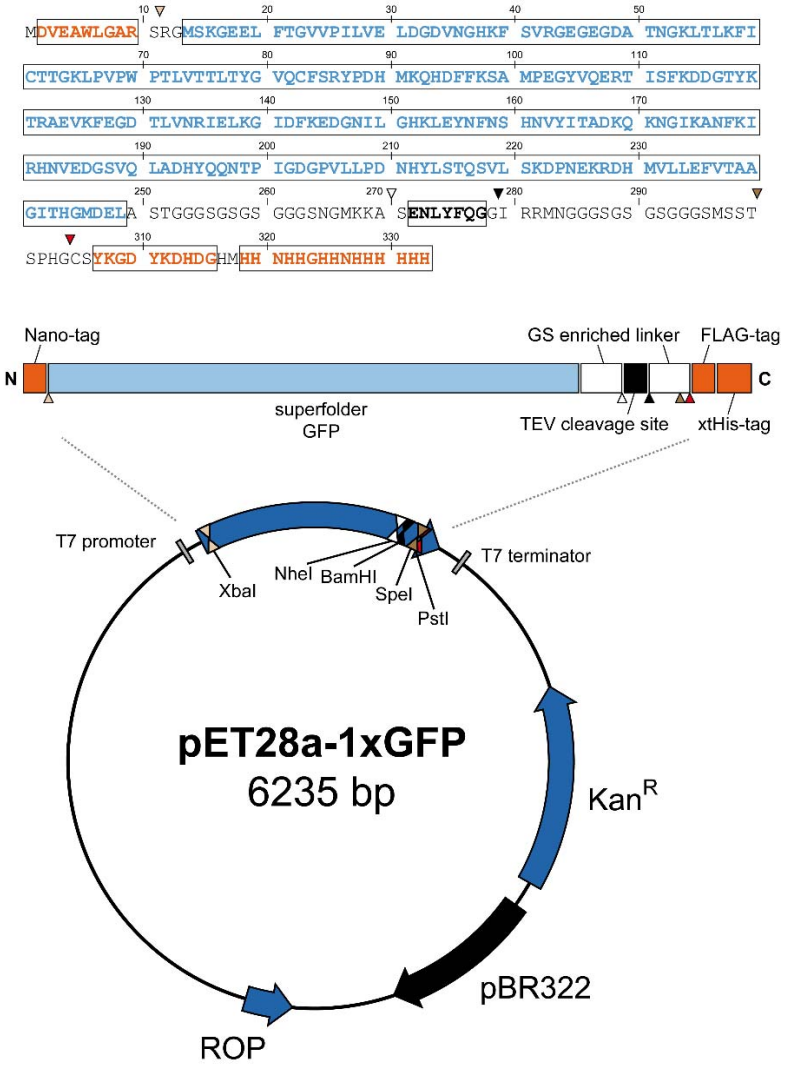

FIGURE S1 1xGFP amino acid sequence and plasmid construct. The 1xGFP construct is based on the pET28a plasmid (Novagene). The plasmid contains a pBR322 origin of replication (black arrow) and three genes (blue arrows), a kanamycin resistance (Kan^R) gene, a gene for the regulator protein Rop to control DNA replication (ROP), and the open reading frame for sfGFP surrounded by a T7 promotor/terminator. The open reading frame code for elements depicted as boxes in this scheme: superfolder GFP (sfGFP; light blue), Nano-/FLAG/xtHis-Tag (orange), glycine/serine-rich flexible linkers (white), and a tabac mosaic etch virus (TEV) cleavage site (black). Sequences coding for these elements are interspaced by distinctive restriction sites depicted as triangles: *Xba*I (beige), *Nhe*I (white), *Bam*HI (black), *Spe*I (ochre), *Pst*I (red). All sfGFP-based constructs in this study were generated in this plasmid background. Plasmids encoding EGFP-based constructs (1) were a kind gift by Ajitha Cristie-David and Neil Marsh, University of Michigan.

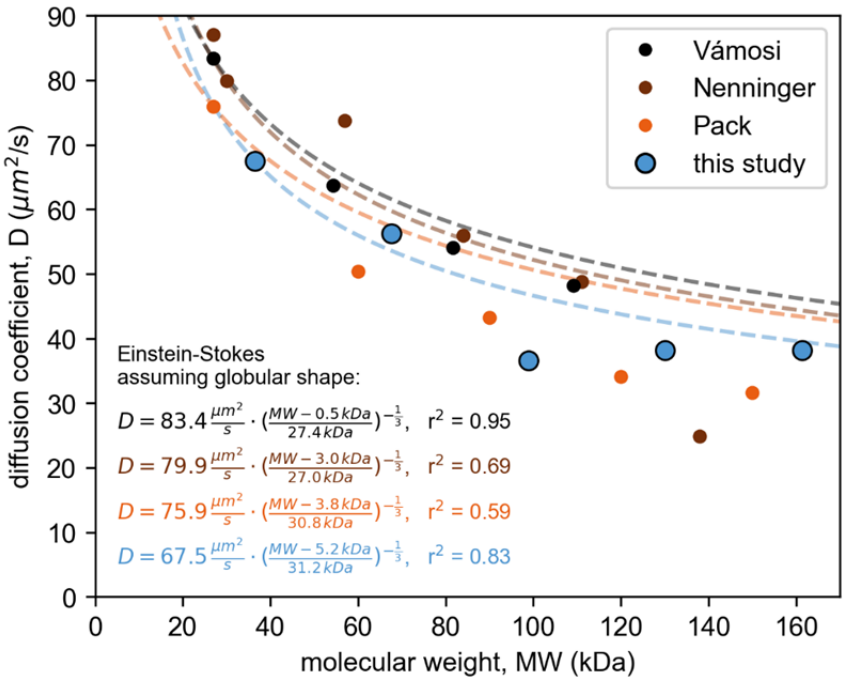

FIGURE S2 The shape of GFP concatemers determined from FCS measurements in solution. Purified sfGFP concatemers (1xGFP, 2xGFP, 3xGFP, 4xGFP, 5xGFP) were diluted to 10 nM in fluorescent-free PBS and the diffusion coefficients were measured using FCS (synchronized pulsed 482 nm excitation and detection with 525/50 emission filter). Note that the diffusion coefficient for sfGFP concatemers decreases with increasing stoichiometry. Similar behaviors of GFP concatemers were described previously (2-4) and are shown for comparison. The data were fitted with the Einstein-Stokes model assuming spherical particles in a classical fluid (inset, Eq. 8 and Eq. 9) where the Einstein-Stokes equation has been modified to account for the different constructs and linkers used (5). The values of Nenninger et al. were measured in cells and are adjusted assuming an 8.9-fold increase in diffusion in water, as seen for their GFP *in vitro* control (3). The deviation of the measured and published data from the Einstein-Stokes model suggests that the shape of the concatemer differs from a perfect sphere.

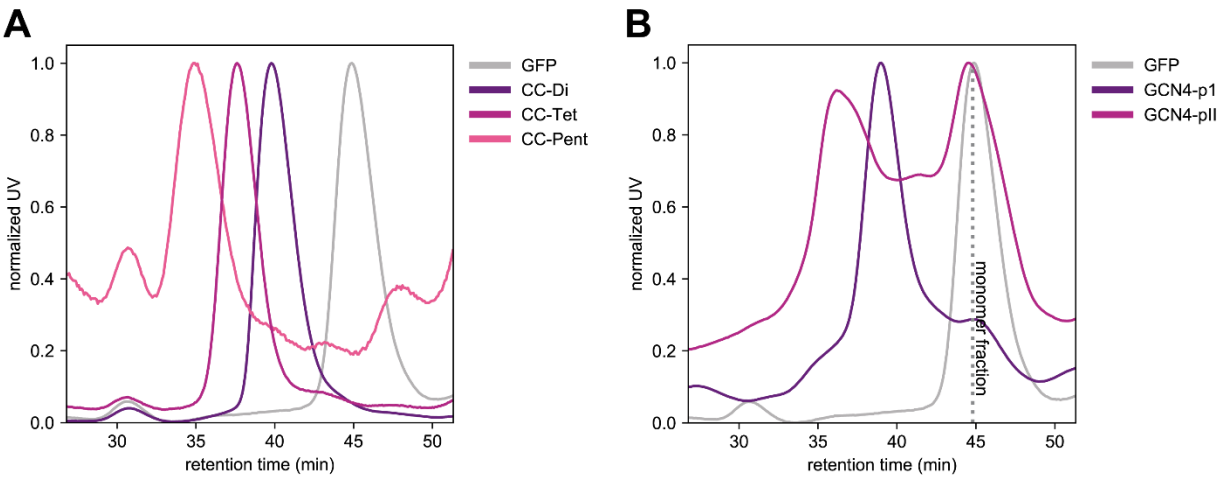

FIGURE S3 Size exclusion chromatography profiles of different GFP-coiled-coil fusion proteins. (*A*) SEC of EGFP-coiled-coil constructs, originally designed by Cristie-David et al. (1) (loading concentrations: GFP, 106 µM; CC-Di, 142 µM; CC-Tet, 101 µM; CC-Pent, 21 µM). (*B*) SEC of EGFP (106 µM), GCN4-p1 (40 µM) and GCN4-pII (20 µM) constructs. In the case of the GCN4 based fusion proteins, the presence of a monomer peak suggests partial dissociation of the GCN4-p1 and GCN4-pII complexes as the separation proceeds on the SEC column. Partial dissociation might originate from the lower loading concentrations of GCN4 fusion proteins (higher concentrations were difficult to obtain). GFP-coiled coil fusion proteins were purified via IMAC and dialyzed against 25 mM HEPES (pH 7.5), 100 mM NaCl, 2 mM EDTA, and 30 % glycerol. The chromatography buffer was identical to the dialysis buffer with the exception that it did not contain glycerol.

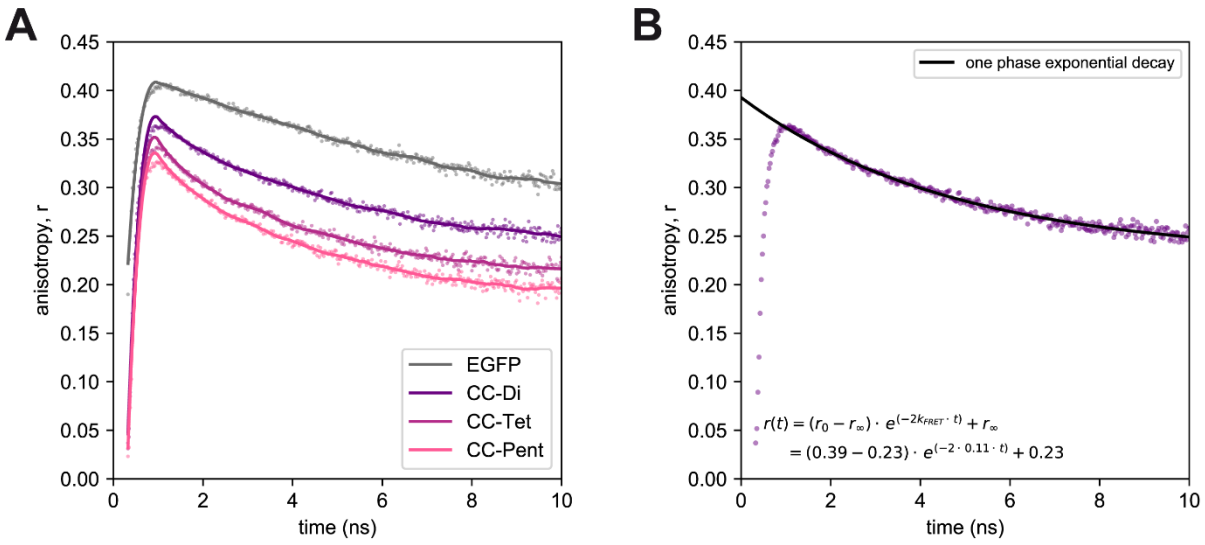

FIGURE S4 Determination of the homotransfer rate k_{FRET} from time-resolved anisotropy decays. (*A*) Time-resolved anisotropy of EGFP-coiled-coil fusion proteins (EGFP, CC-Di, CC-Tri, CC-Pent). The raw data was smoothed using a Savitzky-Golay filter with a window size of 51 bins and a polynomial order of 3. (*B*) The homo-FRET rate k_{FRET} can be derived from the time-resolved anisotropy decay as exemplified by the time-resolved anisotropy data for CC-Di that was fitted with a single-exponential decay function with an offset.

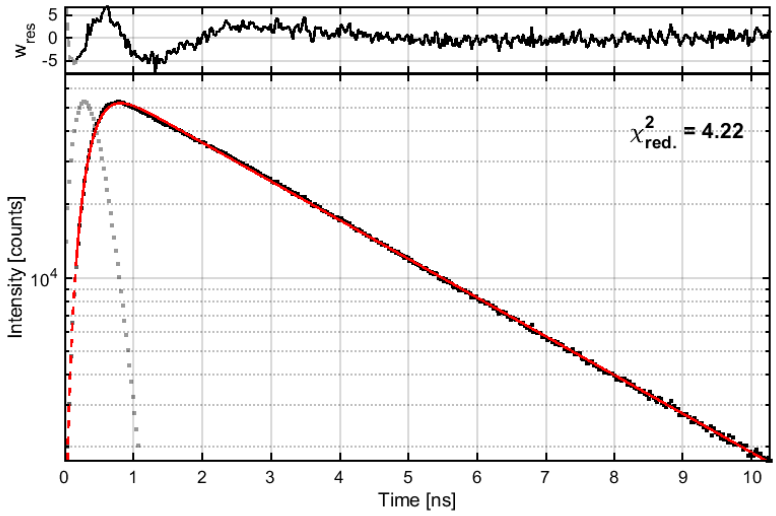

FIGURE S5 Exemplary fit to the fluorescence lifetime decay. The florescence intensity decay for 1xGFP is shown as an example for calculating the lifetime of various GFP fusion proteins used in the study. The dotted grey data points represent the measured IRF of a scattering solution. The measured data points for the GFP sample are shown in black. A mono-exponential fit to the data is shown as a red line. The goodness of a fit was judged using the reduced chi square and weighted residuals for the fit are shown in the top panel.

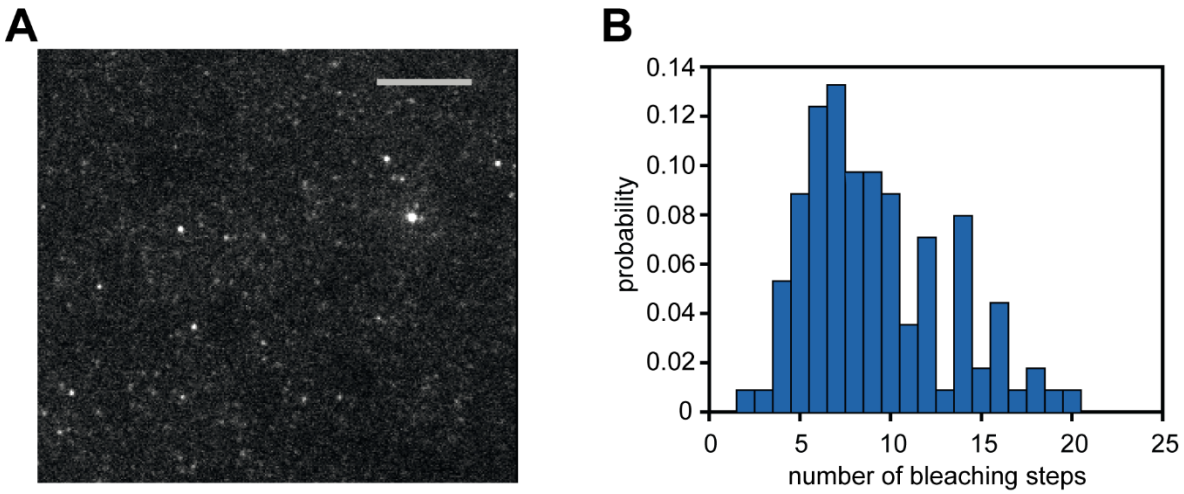

FIGURE S6 TIRF microscopy based direct photobleaching of sfGFP-ph3a. (*A*) A TIRF field of view of surface-immobilized ph3a proteins before photobleaching. (*B*) The distribution of the number of photobleaching steps as analyzed from the different punctae. The distribution has maxima at 7mer and 14mers suggesting each complex is a heptamer with two complexes occasionally occurring within a diffraction-limited spot.

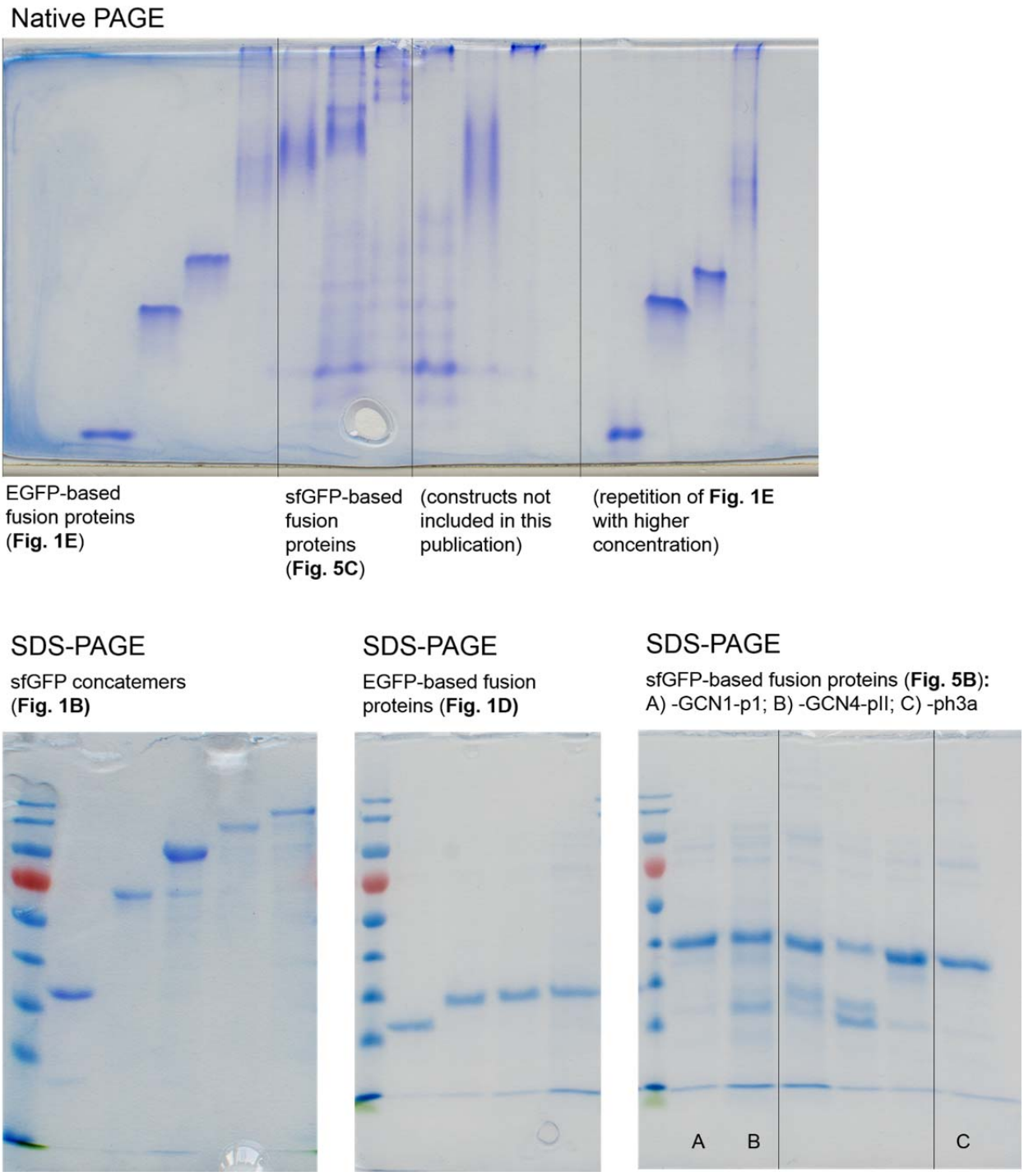

FIGURE S7 Images of polylacrylamide gel representing uncropped versions of images shown in the main text. Those parts that are included in Figs. 1 and 5 of the main manuscript are annotated correspondingly. Note that there is very little evidence of aggregation and degradation. Very minor aggregation can be detected in some lanes in native PAGE (EGFP-CC-Pent, sfGFP-GCN4-pII) where minor fractions of some samples did not migrate into the gel.

Supplementary Tables

TABLE S1 Determination of protein stoichiometry N from fluorescence anisotropy using construct-specific versus crosswise standardized parameters.

	$N_{SS,std}$		$N_{x,a}$	
Fusion protein	(sfGFP-based parameter set)	(EGFP-based parameter set)	a = 0.10	a = 0.21
1xGFP	1.0	(0.9)	1.0	(1.0)
2xGFP	2.0	(1.3)	1.9	(1.6)
3xGFP	3.1	(1.9)	2.7	(2.1)
4xGFP	3.1	(1.9)	2.9	(2.2)
5xGFP	2.9	(1.8)	2.8	(2.2)
EGFP	(1.2)	1.0	(1.0)	1.0
EGFP-CC-Di	(3.6)	2.1	(2.9)	2.3
EGFP-CC-Tet	(5.9)	3.1	(3.7)	2.7
EGFP-CC-Pent	(5.9)	3.1	(3.5)	2.7

( ) Calculations with the parameter set / parameter a of the opponent fusion protein system (EGFP parameters for sfGFP, and vice versa).

TABLE S2 Diffusion coefficients of sfGFP-GCN4-p1 and sfGFP-GCN4-pII constructs.

Protein	oligomeric state	Molecular weight (kDa)	Time of the measurement (min)	Diffusion coefficient, D ($\mu m^2 s^{-1}$)
GCN4-p1	2	77	2	34.1
			90	31.5
GCN4-pII	3	116	2	24.7
			90	21.8

Supplementary Theory

A) Fractional Photobleaching

Yeow and Clayton's model (6) describes the fluorescence anisotropy $r_{SS}(x,N)$ of an oligomer with N subunits that interact via homo-FRET as a function of fractional photobleaching:

$$\begin{aligned} r_{SS}(x, N) &= r_1 \cdot \left(f_{non} + \left(1 - f_{non}\right) \cdot x^{(N-1)}\right) = \\ &= r_1 \cdot f_{non} + r_1 \cdot (1 - f_{non}) \cdot x^{(N-1)} \end{aligned} \tag{S1}$$

with r_1 as the anisotropy of the monomer, f_{non} as the fraction of non-interacting fluorophores, N as the number of interacting subunits in a homo-FRET cluster, and x as the fraction of non-fluorescent subunits. Eq. (S1) equals Eq. 5 from the Theory section of the main manuscript.

In Eq. S1, the steady-state anisotropy of fractionally photobleached samples relies on the parameter f_{non}, which is visualized in Figure S8. As the anisotropy of complexes with more than one label is assumed to be zero in Yeow and Clayton, the steady-state anisotropy of fully labeled (i.e. unphotobleached samples, where x equals zero), solely depends on f_{non}

$$\mathbf{r_{SS}(f_{non}) = r_1 \cdot f_{non}} \ . \tag{S2}$$

This approximation may work for partial labeling experiments at low labeling density for which the theory was developed. However, for 100 % labeling efficiency, the typical starting point for photobleaching experiments, only the monomer term survives. Hence, we interpret this first term as $\mathbf{r_1 \cdot f_{non}}$ as the unphotobleached steady-state anisotropy. We then rewrite Eq. (S1) as:

$$\begin{aligned} r_{SS}(x, N) &= \mathbf{r_1 \cdot f_{non}} + \mathbf{r_1} \cdot (\mathbf{1 - f_{non}}) \cdot x^{(N-1)} = \\ &= \mathbf{r_{SS}(f_{non})} + \mathbf{\Delta r_{SS}(f_{non})} \cdot x^{(N-1)} \end{aligned} \tag{S3}$$

where $\Delta r_{SS} = r_1 - r_1 \cdot f_{non}$.

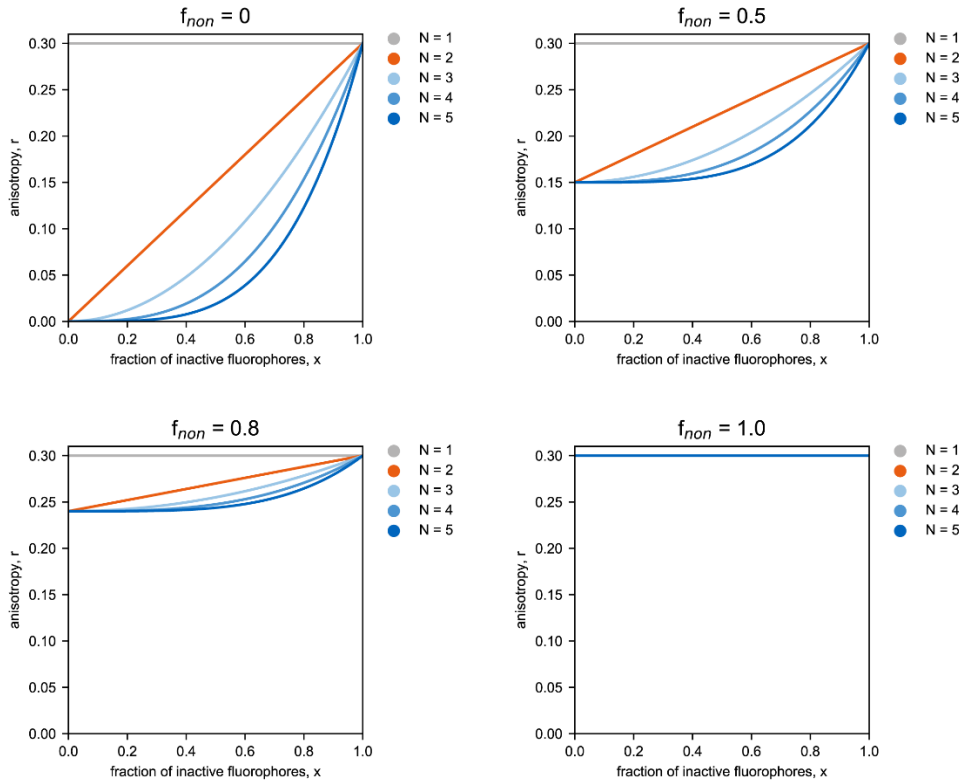

FIGURE S8 In the Yeow and Clayton model, the anisotropy of fractionally photobleached samples depends on f_{non}. The graphs show data generated with Eq. S1 and parameters r_1 = 0.3 and N = 1, 2, 3, 4, 5. The fraction of inactive fluorophores x was varied from 0 to 1.

We then exchanged $r_{SS}(f_{non})$ with $r_{SS}(N) = r_1 \cdot \frac{(1+a)}{(1+N \cdot a)}$:

$$r_{SS}(x, N) = r_{SS}(N) + \left(r_1 - r_{SS}(N)\right) \cdot x^{(N-1)},$$
$$r_{SS}(N) = r_1 \cdot \frac{(1+a)}{(1+N \cdot a)} \qquad \text{(S4)}$$

where r_1 is the monomer anisotropy.

The term $r_{SS}(N) = r_1 \cdot \frac{(1+a)}{(1+N \cdot a)}$ comes from equation 18 of the original publication by Runnels and Scarlata [7], where the anisotropy of complexes that have undergone homoFRET is assumed to be zero (i.e. $r_{ET} = 0$). It reflects the inverse proportional character of r_{SS} on increased number of interacting fluorophores N. We replaced the product of the energy transfer rate k_{FRET} (parameter *F* in [7]) and the fluorescence lifetime τ in Runnels and Scarlata's derivation with *a*,

which we then determine empirically. This minimizes the usage of parameters determined from time-resolved anisotropy measurements and allowed us to interpret the steady-state anisotropy data only by the use of reference molecules.

For a better intuitive understanding of formula (S4), the terms of the equation are isolated. The green part of the equation determines the anisotropy coming from non-photobleached molecules\ (Fig. S9):

$$r_{SS}(x, N) = r_{SS}(N) \tag{S5}$$

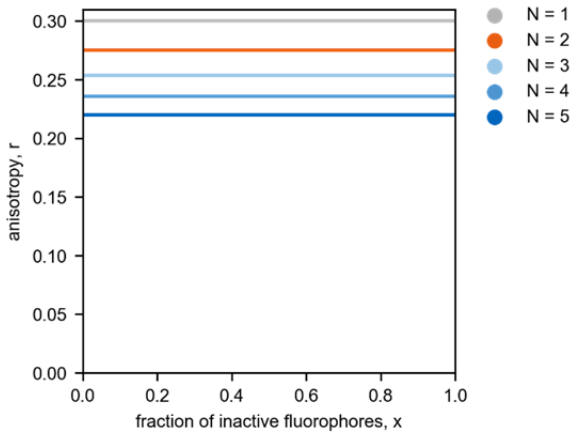

FIGURE S9 Visualization of Eq. (S5) as the first part of Eq. (S4). In our model, Eq. (S5) describes the steady-state anisotropy without photobleaching. The theoretical values were calculated by assuming $r_1 = 0.3$ and $a = 0.1$.

The anisotropy is constant, only the fraction of unphotobleached molecules contributing to the total anisotropy changes with photobleaching.

The purple portion describes the change in anisotropy due to photobleaching. As in Yeow and Clayton, only the complexes containing one fluorophore contribute, and this fraction depends on how many subunits are in a complex and increases as with photobleaching (Fig. S10):

$$r_{SS}(x, N) = \left(r_1 - r_{SS}(N)\right) \cdot x^{(N-1)} \tag{S6}$$

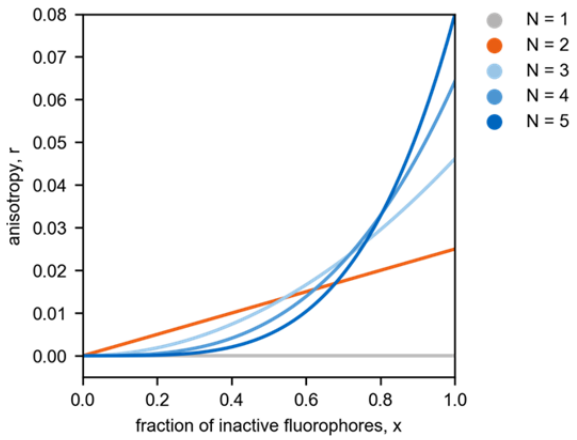

FIGURE S10 Visualization of Eq. (S6) for a growing fraction of photobleached samples. The theoretical values were calculated by assuming $r_1 = 0.3$ and $a = 0.1$.

In this form, the anisotropy increases from the value for fully labeled complexes to end maximally at the monomer level (Fig. S11):

$$r_{SS}(x, N) = r_{SS}(N) + \left(r_1 - r_{ss}(N)\right) \cdot x^{(N-1)} \qquad \text{(S7)}$$

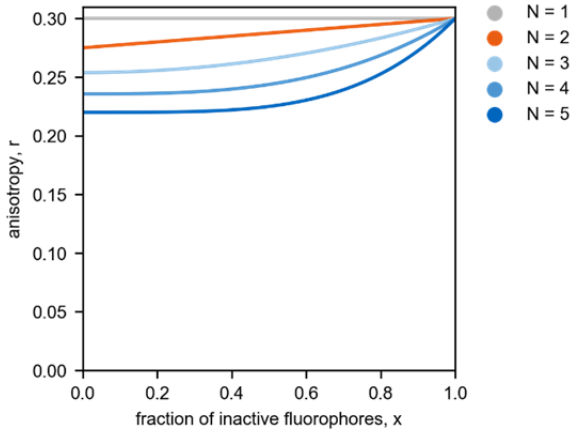

FIGURE S11 Visualization of Eq. (S7) for a growing fraction of photobleached samples. The theoretical values were calculated by assuming $r_1 = 0.3$ and $a = 0.1$.

B) Heterogeneous Oligomeric Samples

Often, biomolecules exist in an equilibrium of complexes with different stoichiometries. We can treat such a heterogeneous system by defining the distribution of monomers υ_1, of dimers υ_2, of trimers υ_3, and so on where υ_i represents the fluorescence intensity of the i^{th} species. The distribution of the different species can vary between 0 and 1, but the total must sum up to 1.

For multiple components, the total anisotropy is given by the sum of the components multiplied by their fractional intensity. Hence, we can describe the anisotropy behavior of a heterogeneous system upon fractional photobleaching, x, as a sum of distributions multiplied with their respective $r_{SS}(x, N)$. In an exemplary case where we assume a mixture of monomers, dimers, and trimers (with υ_1, υ_2, and υ_3), the model is represented by Eq. (S8):

$$\begin{aligned} r_{SS}(x, \upsilon_1, \upsilon_2, \upsilon_3) &= \upsilon_1 \cdot r_{SS}(x, N{=}1) + \upsilon_2 \cdot r_{SS}(x, N{=}2) + \upsilon_3 \cdot r_{SS}(x, N{=}3) = \\ &= \upsilon_1 \cdot (r_1) + \\ &+ \upsilon_2 \cdot \left(r_1 \cdot \frac{1+a}{1+2\cdot a} + r_1 \cdot x - r_1 \cdot \frac{1+a}{1+2\cdot a} \cdot x\right) + \\ &+ \upsilon_3 \cdot \left(r_1 \cdot \frac{1+a}{1+3\cdot a} + r_1 \cdot x^2 - r_1 \cdot \frac{1+a}{1+3\cdot a} \cdot x^2\right) \end{aligned} \tag{S8}$$

Based on our model, we can theoretically calculate the behavior of mixed samples upon fractional photobleaching, as shown in Figure S12. As we are only interested in determining whether it is possible, in principle, to distinguish between different distributions, we ignore the fact that the photobleaching probability is most likely different for the various complexes. In the case of the 0.5 monomer | 0.5 trimer mixture (Fig. S12 D), the behavior deviates from that of a homogeneous dimer sample (Fig. S12 A), thus indicating that a mixture of monomers and trimers results in anisotropy that is clearly different from that of a dimer. When comparing the behavior of the 0.5 monomer | 0.5 trimer mixture to the 0.3 | 0.3 | 0.3 mixture (Fig. S12 E), though, both curves are difficult to distinguish.

In summary, the predicted behaviors of heterogeneous oligomer mixtures as a function of fractional photobleaching do depend on their composition. However, to distinguish between these behaviors experimentally, one would require highly resolved steady-state anisotropy data (r_{SS} errors around ±0.005) that may be difficult to obtain, according to our experience.

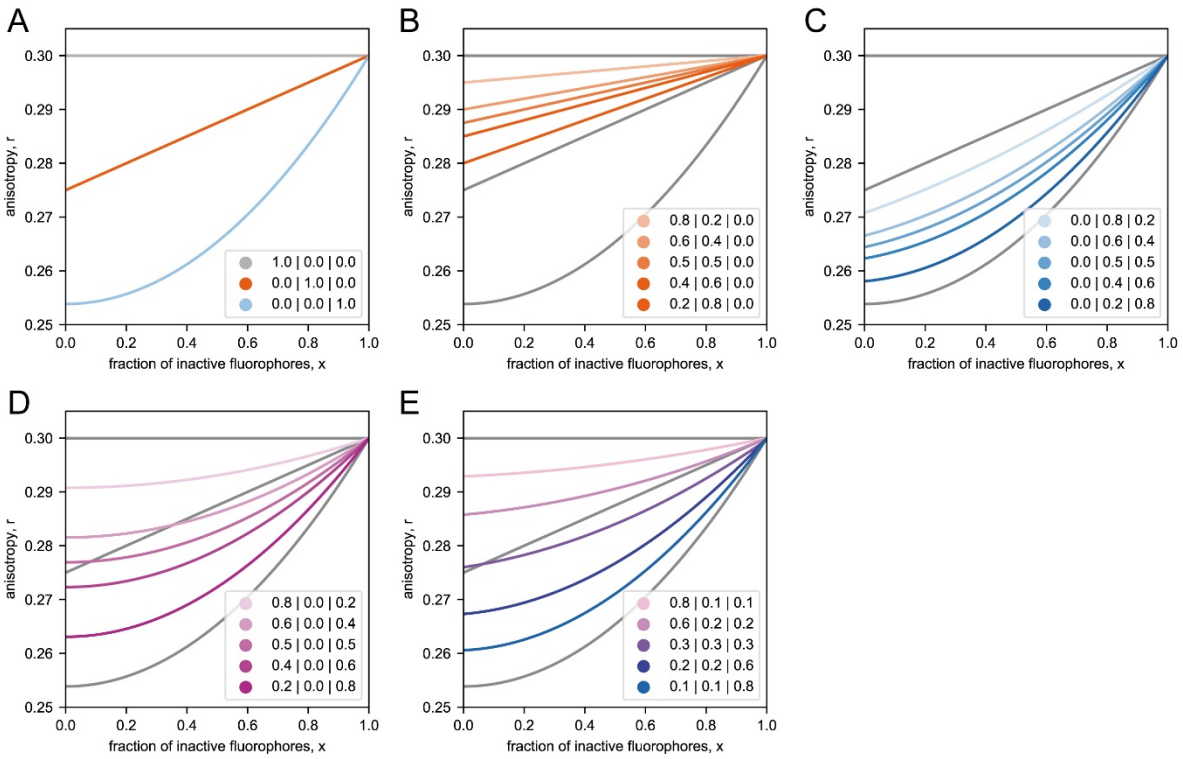

FIGURE S12. Theoretical anisotropy behavior of heterogeneous GFP monomers, dimer, and trimers upon photobleaching. The distribution of species is displayed as (monomer fraction υ_1 | dimer fraction υ_2 | trimer fraction υ_3). **A)** Hypothetical behavior of monomers (grey), a homogeneous dimer (orange), and a homogeneous trimer (blue) upon photobleaching. The behaviors were calculated for $x \rightarrow 1$ with eq. (S8), assuming $r_1 = 0.3$ and $a = 0.1$ (similar to values determined for sfGFP concatemers). Theoretical behavior of monomer / dimer mixtures (**B**), of dimer / trimer mixtures (**C**), of monomer / trimer mixtures (**D**), and of monomer, dimer, and trimer mixtures (**E**). The homogeneous samples from **A** are displayed in grey as a reference.

Supporting References

1. Cristie-David, A. S., A. Sciore, S. Badieyan, J. D. Escheweiler, P. Koldewey, J. C. A. Bardwell, B. T. Ruotolo, and E. N. G. Marsh. 2017. Evaluation of de novo-designed coiled coils as off-the-shelf components for protein assembly. Molecular Systems Design & Engineering 2(2):140-148. 10.1039/C7ME00012J.
2. Vámosi, G., N. Mücke, G. Müller, J. W. Krieger, U. Curth, J. Langowski, and K. Tóth. 2016. EGFP oligomers as natural fluorescence and hydrodynamic standards. Scientific Reports 6:33022.
3. Nenninger, A., G. Mastroianni, and C. W. Mullineaux. 2010. Size dependence of protein diffusion in the cytoplasm of Escherichia coli. Journal of Bacteriology 192(18):4535-4540. Article.
4. Pack, C., K. Saito, M. Tamura, and M. Kinjo. 2006. Microenvironment and effect of energy depletion in the nucleus analyzed by mobility of multiple oligomeric EGFPs. Biophys. J. 91(10):3921-3936.
5. Einstein, A. 1905. Über die von der molekularkinetischen Theorie der Wärme geforderte Bewegung von in ruhenden Flüssigkeiten suspendierten Teilchen. Annalen der Physik 322(8):549-560.
6. Yeow, E. K. L., and A. H. A. Clayton. 2007. Enumeration of oligomerization states of membrane proteins in living cells by homo-FRET spectroscopy and microscopy: Theory and application. Biophysical Journal 92(9):3098-3104.
7. Runnels, L. W., and Suzanne F. Scarlata. 1995. Theory and application of fluorescence homotransfer to melittin oligomerization. Biophysical Journal, 69(4), 1569–1583.